



Structural changes induced in thionins by chloride anions as determined by molecular dynamics simulations

Svetlana V. Oard^{a,*}, Frederick M. Enright^b, Bin Li^c

^a AgCenter Biotechnology Laboratory, Louisiana State University, Baton Rouge, LA, United States

^b Department of Veterinary Science, Louisiana State University, Baton Rouge, LA, United States

^c Department of Experimental Statistics, Louisiana State University, Baton Rouge, LA, United States

ARTICLE INFO

Article history:

Received 4 November 2009

Received in revised form 21 December 2009

Accepted 23 December 2009

Available online 4 January 2010

Keywords:

Antimicrobial peptides

Anions

Membrane permeabilization

β -purothionin

α -hordothionin

Thionins

ABSTRACT

Computational analysis of two membrane-permeabilizing peptides, barley α -hordothionin and wheat β -purothionin, revealed that anions can trigger dynamic and structural changes in the thionin antiparallel double α -helix core. Analysis of the molecular dynamics simulations demonstrated that anions induced unfolding of the $\alpha 2$ and $\alpha 1$ helices at the carboxyl ends which are located on the opposite ends of the α -helix core. An internalized water molecule was observed inside the unfolded $\alpha 2$ C-end. Strong interactions of anions with the R30 regulating network or simultaneous interactions of anions with the phospholipid-binding site and the R30 hydrogen bonding network triggered unfolding of the $\alpha 2$ C-end. An increase of anion density for two residues of the phospholipid-binding site (K1, R17, and Q22) or R17 and R19 and a preceding unfolding of the $\alpha 2$ C-end were necessary for unfolding of the $\alpha 1$ C-end. Anions interacted primarily with residues of the phospholipid-binding site and the R30 network while the $\alpha 1/\alpha 2$ hydrophobic region was void of anions. However, during strong interactions of anions with the R30 network and phospholipid-binding site, the $\alpha 1/\alpha 2$ hydrophobic region attracted anions which interacted with conserved residues of the $\alpha 1$ C-end. Analysis of anion-induced rearrangements pointed to auxiliary residues of the R30 network and the phospholipid-binding site. Induction of conformational changes on the opposite ends of the α -helix core by interactions of anions with the phospholipid-binding site may be relevant to a mechanism of membrane-permeabilizing activity.

Published by Elsevier B.V.

1. Introduction

Thionins belong to a family of highly basic plant antimicrobial peptides with broad spectrum antibacterial and antifungal activities [1–3]. They exhibit indispensable characteristics for developing new antibacterial and antifungal drugs: a broad range of activity, low minimal inhibitory concentrations, and rapid mode of action. Because thionins act by permeabilizing microbial membranes, there is less likelihood that target microbes will develop resistance to these peptides [3–6]. Microbial growth inhibition mechanisms of thionins as well as linear antimicrobial peptides demonstrate interaction with phospholipids to cause membrane instability [7–10]. Fungal or bacterial growth inhibition correlates with membrane-permeabilizing activity for both linear amphipathic antimicrobial peptides and thionins [11–13]. This evidence indicates that membrane permeabilization is very important for inhibiting growth of microorganisms.

While several hypotheses have been proposed [1,3,10], the mechanism of membrane permeabilization by thionins remains to be solved.

Thionins are 45–47 amino acids long, highly basic, and resistant to various environmental conditions [3,14]. Secondary structure of thionins is conserved and consists of a β -sheet and an antiparallel double α -helix core bound by three or four disulfide bridges (see Fig. S1 in the Supporting Information). Crystallographic data indicate the presence of the phospholipid-binding site in the groove formed by the arm and stem at the inner corner of the global Γ fold of thionins [3,15,16]. The main contributors of the phospholipid-binding site include K1, S2, R10, Y13, and R17, which are highly conserved in the thionin family [3,17].

Based upon numerous *in vitro* experiments, thionins permeabilize the bacterial, fungal, mammalian, and plant membranes under low ionic conditions [3,9]. Thionins bind to the membrane components, e.g. the negatively charged phospholipid phosphatidyl serine, which is present in bacterial, fungal, mammalian, and plant membranes. In model unilamellar vesicle studies, thionins permeabilize membranes only when the vesicles contain negatively charged phospholipids [18]. A thionin from *Pyrularia pubera* (PpTH) binds to phosphatidyl serine and phosphatidic acid, and effectively solubilizes these negatively charged phospholipids into the aqueous phase from the organic

* Corresponding author. LSU AgCenter Biotechnology Laboratory, Louisiana State University, 115 Wilson Bldg., LSU, Baton Rouge, LA, 70803, United States. Tel.: +1 225 578 7865; fax: +1 225 578 7863.

E-mail address: soard@agctr.lsu.edu (S.V. Oard).

phase, suggesting the formation of a proteolipid complex [3]. Thionins insert into the membrane bilayer modifying the lipid packing [5,9]. The electrostatic interactions are followed by hydrophobic interactions. The existence of electrostatic interactions between the peptide and the membrane bilayer was demonstrated for the thionin from *Pyricularia pubera* (PpTH) [19] and β PTH [5] by two different methods. However, no details on effects of electrostatic interactions on thionins and contribution to the membrane-permeabilizing capability were offered to date.

The toxicity of purothionins may be based on the formation of ion channels in membranes [7]. Purothionins form cation-selective ion channels in artificial lipid bilayers and in the plasmalemma of rat neurons. Membrane composition affected properties of ion channels, with phosphatidyl serine increasing channel activity. Interactions of β -purothionin (β PTH) [6,17,20] with the model membranes were also consistent with protein channel formation, rather than membrane disruption [5,9]. In contrast, fluorescent probes, which could not move through ion channel pores, were released from lipid vesicles in the presence of α -purothionin suggesting destabilization and disruption of the membrane [18]. Another proposed model for membrane permeabilization by thionins is based on the ability to solubilize negatively charged phospholipids [3]. In this model, thionins bind to negatively charged phospholipids and then withdraw phospholipids causing solubilization of the membrane.

A minimal motif in thionins retaining antimicrobial activity, as determined by testing several truncated PpTH peptide derivatives, consisted of only the double α -helix core [21]. The minimal motif included the conserved residues R10, Y13, and R17, which belong to the phospholipid-binding site [3]. Recently, molecular dynamics (MD) simulations of β PTH and α -hordothionin (α HTH) from barley endosperm [22–24] revealed that a portion of the double α -helix core, the C-end of the α 2 helix, is highly dynamic [25,26]. Dynamic modulation of the α 2 C-end is regulated by the R30 hydrogen bonding network. The R30 networks in β PTH and α HTH are D42-K5-R30-N27 and G42-R5-R30-G27, respectively, and similar networks are found in other thionins [26]. They contain two basic residues in the middle that are tightly bound to each other by two disulfide bonds (Fig. S1). When the R30 network is perturbed, the repulsive interactions between R30 and R5/K5 side chains create structural perturbations which are passed to the α 2 C-end, and the later unfolds. These results encourage further investigation because a transmembrane α -helical bundle has been associated with formation of pores and membrane permeabilization by cationic linear peptides [10,27,28].

In this work, we report the systematic investigation of the β PTH and α HTH MD trajectories to better understand factors inducing conformational changes in the α -helix core. Analyses of multiple characteristics revealed that negatively charged anions induce conformational perturbations on the opposite ends of the α -helix core, at the carboxyl ends of the α 1 and α 2 helices. Structural perturbations in the α -helix core were observed upon interactions of anions with the R30 regulating network and/or the phospholipid-binding site. These data suggest that interactions of thionins with negatively charged phospholipids are not limited to attractive electrostatic interactions, but also induce structural changes in the α -helix core.

2. Methods

2.1. Dynamic modulation of the α -helix core

The objective of this work was to investigate cause(s) of dynamic modulation of the α -helix core which persisted in MD simulations of two thionins, β PTH and α HTH, under three different conditions (Cl^- anions, Cl^- anions + K^+ cations, and Cl^- anions + Mg^{+2} cations) [25,26]. Main structural fluctuations were observed at the carboxyl ends of the α 2 and the α 1 helix in each of six MD simulations (Fig. S2). The main focus of this study was to understand frequently observed structural perturbations of

the α 2 C-end which continued predominantly for 1–2 ps and consisted of significant changes of the backbone dihedral angles for residues N27/G27 and V28, loss of hydrogen bonds, α -helix/coil transition, and increases of distances between up to six residues. Because unwinding of the α -helical secondary structure was observed among other structural changes, we refer to this dynamic modulation as a α 2 C-end unfolding event. In contrast, the α 1 C-end frequently underwent extensions that continued predominantly for 1–10 ps and consisted of forming hydrogen bonds and coil/ α -helix transition elongating the α 1 C-end by three residues. Rarely, dynamic modulation of the α 1 C-end resembled that of the α 2 C-end that included significant changes of the backbone dihedral angles for residues L15 and C16, loss of hydrogen bonds, α -helix/coil transition, and an increase of distances between four residues. These perturbations are designated as a α 1 C-end unfolding event.

2.2. Computational methods

Numerous α 2 C-end unfolding events were observed in each of six MD trajectories. Therefore, the β PTH and α HTH MD simulations with Cl^- anions only were selected for this study as the simplest systems among the above six simulations. The unconstrained all-atom MD simulations of β PTH and α HTH in explicit water were performed and analyzed previously [25,26]. Briefly, atomic parameters used to describe all atoms were taken from the Amber99 force field library [29], and the flexible, single point charge (fSPC) water potential [30] was used to describe water. The fSPC water model was chosen even though it is computationally more expensive because this model was shown to perform better than the rigid point charge models such as TIP3P [31], SPC/E [32], and TIP4P_{EW} [33] when modeling Cl^- anions [34,35]. To increase reliability of computations, both the fSPC and Cl^- parameters were taken from the same force field library. The initial structure of β PTH was obtained from the X-ray structure of Stec et al. (1995) with a PDB entry code 1BHP [16]. The initial α HTH structure was obtained from the X-ray structure of barley β -hordothionin with a PDB entry code 1WUW by changing six residues N27G, A28V, G36S, L37S, S41T, and S42G using the AMBER-8 software package. The simulation box was neutralized by adding 9 and 10 Cl^- ions to β PTH and α HTH, respectively. MD simulations were performed using the Peach 5.8 software package [36], in periodic boundary conditions and the canonical ensemble. The long-range Coulomb forces were calculated using the particle mesh Ewald method [37]. Optimization of simulation parameters was performed to achieve sufficient accuracy with the relative average root mean square fluctuation (RMSF_r) of total energy $\leq 0.1\%$. No bond length constraints were applied to obtain high precision calculations. Preceded by minimization and 1 ns-long equilibration of the system, the production runs were performed at 300 K for 2 and 5 ns for β PTH and α HTH, respectively.

Analysis of the MD trajectories was performed using Peach 5.8 [38] and Amber-8 [39]. VMD1.8.6 [40] was used for visualization of the trajectories. Secondary structures were defined with the DSSP program [41]. A hydrogen bond was defined by donor–acceptor distance smaller than 3.0 Å and donor–hydrogen–acceptor angle larger than 135°. Convergence of the MD trajectories, root mean square difference for all heavy atoms, and backbone atoms, as well as root mean square fluctuation, average solvent-accessible area (SAA), and hydrogen bonds were reported previously [25,26]. Because the α HTH and β PTH MD trajectories converged at approximately 1500 and 600 ps, the first 2 ns and 1 ns were omitted for the analysis of the α HTH and the β PTH MD trajectory, correspondently.

2.3. Statistical analysis of dynamic modulation of the α 2 C-end

A total of 38 characteristics were selected to study correlations with unfolding of the α 2 C-end including structural changes and interactions with water in different structural regions of the peptides

(Table 1). Residues of the R30 hydrogen bonding network were included because our previous results suggested association of the R30 network with the $\alpha 2$ C-end unfolding [25,26]. An unfolding event for the $\alpha 2$ C-end was represented by breakage of the L24-O:V28-N hydrogen bond as deduced from the time evolution.

The statistical approach employed to investigate the time-dependent relationship between the Leu24-O:V28-N hydrogen bond status change and 38 peptide structure-related parameters was based on Multiple Additive Regression Trees (MART), originally proposed by Friedman [42]. MART is one of several techniques that aim to improve the performance of a single model by fitting many models and combining them for prediction. MART uses two algorithms: “trees” are from the Classification and Regression Tree (CART) [43] and “boosting” builds and combines a collection of models, i.e. trees. Boosting improves model accuracy, based on the idea that it is easier to find and average many rough rules of thumb, than to find a single highly accurate prediction rule [44]. In boosting, models (e.g., decision trees) are fitted iteratively to the training data, using appropriate methods to gradually increase emphasis on observations modeled poorly by the existing collection of trees. Besides its exceptionally high prediction accuracy, MART can estimate the relative influence of predictor variables based on the number of times a variable is selected for splitting, weighted by the improvement to the model as a result of each split, and averaged over all trees.

All hydrogen bonds including the dependent variable, the L24-O:V28-N hydrogen bond, were treated as categorical values where 1 and 0 corresponded to the formation or breakage of a hydrogen bond. First, MART models were fitted and twelve predictors were identified based on their relative variable influence using the entire dataset (all time steps). Then fitting of the MART models was repeated considering only the steps when unfolding events occurred and 4 preceding steps before breakage of the L24-O:V28-N hydrogen bond. Thus, a 2 ps-long time interval was analyzed before each unfolding event.

2.4. Analysis of series of unfolding events in the α HTH MD trajectory

To increase the time interval before an unfolding event, only series of the $\alpha 2$ C-end unfolding events were analyzed. The time interval between two consecutive unfolding events for the $\alpha 2$ C-end ranged from 1 to 140 ps in the β PTH and α HTH MD trajectories. Therefore, some of 2 ps-long time intervals in the statistical analysis contained a

preceding unfolding event. To circumvent this problem, further analysis was performed on the α HTH MD trajectory, which contained eight independent series of the $\alpha 2$ C-end unfolding events between 2 and 5 ns. Each series was considered independent because the adjacent series showed significant conformational differences (at least for 10% of residues following the criteria described below) and large variation of coordinates for Cl^- anions. Each series consisted of two or more unfolding events and was separated by at least 110 ps intervals from a preceding and a following series. Use of series allowed increasing a preceding time interval to 100 ps without the problem of overlapping with a preceding unfolding event.

The presence of eight independent series of unfolding allowed us to use this trajectory for analysis of the $\alpha 2$ C-end unfolding series. Although it is true that even a 100 ns-long equilibration may be insufficient for certain proteins to converge [45], a required length of simulation depends on intrinsic properties of a protein and the characteristic under study. Eight independent series of unfolding were observed between 2 and 5 ns in α HTH MD trajectory. The intrinsic properties of α HTH combine a small size with four disulphide bonds enforcing a highly knotted structure and 10 basic residues contributing to a relatively high frequency of dynamic fluctuations which was observed in all MD simulations of β PTH and α HTH [25,26].

Reduction of number of preceding time intervals to be analyzed to eight allowed us to expend analysis of associations with the $\alpha 2$ C-end unfolding. More than 300 characteristics (distances, hydrogen bonds, secondary structures, dihedral backbone angles, side-chain rotamers, SAA for backbone atoms and side chains) were analyzed. The time-dependent relationships between the $\alpha 2$ C-end unfolding and approximately 300 characteristics were analyzed using the time evolution computed for each characteristic. An unfolding event for the $\alpha 2$ C-end was determined from α -helix/coil transition of the secondary structure and perturbations of the φ and ψ backbone dihedral angles (φ , ψ) of the $\alpha 2$ C-end residues, G27 and V28. G27 and V28 existed primarily in the (-75° , -55°) and (-70° , -15°) conformations, respectively [26]. Upon the $\alpha 2$ C-end unfolding, the G27 φ changed to -130° or the G27 ψ and V28 φ switched to 0° and -120° , respectively. Hydrogen bonds were treated as categorical values to indicate the presence or absence of a hydrogen bond. When analyzing torsion angles, changes above 25° and 60° were considered as significant for the backbone angles (φ , ψ) and the side-chain angles (χ_1 , χ_2), respectively. Changes in SAA values for buried residues greater than 2 \AA^2 were considered significant as well as values greater than 15 and 30 \AA^2 for main-chain and side-chain atoms of surface residues, respectively. The ion interaction energy (E_{ion}) was calculated between all atoms of a residue and all Cl^- ions. When analyzing E_{ion} , changes above 5 Kcal/mol were considered significant for all residues except the amide and ionized residues. Changes in E_{ion} above 10 and 30 Kcal/mol were set as significant for amide (N, and Q) and ionized (K, R, D, and E) residues. All characteristics were analyzed within two time intervals before each unfolding series. The first interval (designated as the beginning of unfolding) consisted of 6 ps preceding the first unfolding event in an unfolding series. The second interval (designated as an interval within 100 ps before unfolding) included time steps from 100 to 6 ps prior to the first unfolding event.

To obtain the representative structures before and after the $\alpha 2$ C-end unfolding at 4090 ps, 100 equally spaced snapshots between 2000 and 3600 ps and between 4260 and 5000 ps were averaged, and the snapshots with similar structure to the averaged one were selected.

3. Results

3.1. Unfolding of the C-end of the $\alpha 2$ -helix in β PTH and α HTH

Here we present further analysis of the β PTH and α HTH MD simulations from a series of recently reported six MD simulations [25,26] to understand the nature of dynamic modulations of the C-end

Table 1
Characteristics analyzed in β PTH and α HTH using the statistical approach to study unfolding of the $\alpha 2$ C-end.

	Characteristics analyzed	Localization
Hydrogen bonds	T34-O:K1-N, K1-O:T34-N	B-sheet
	C16-O:G20-N	$\alpha 1$ C-end + L1
	A21-O:L24-N, A21-O:C25-N	$\alpha 2$ N-end
	Q22-O:A26-N, A26-O:C31-N	$\alpha 2$ C-end
	R30-O:K5-NZ(R5-NE) ^a , N(G)27-O:R30-N	R30 network
Dihedral backbone angles (ψ)	C31	B-sheet
	L15, R17	$\alpha 1$ C-end + L1
	K23	$\alpha 2$ N-end
	N(G)27, C29	$\alpha 2$ C-end
	K(R)5, R30	R30 network
	S(K)38	Other
	SAA ^b	K1, C31, L33
S6, T7	$\alpha 1$ N-end	
Y13, L15, R17, R19	$\alpha 1$ C-end + L1	
K23, L24	$\alpha 2$ N-end	
A26, N(G)27, V28, C29	$\alpha 2$ C-end	
R30, K(T)41	R30 network	
G(S)36, S(K)38, K45	Other	

^a Residues varying in the α HTH sequence are shown in parenthesis.

^b Solvent assessable area of the backbone atoms.

in the $\alpha 2$ helix. Numerous unfolding events which lasted 0.4 ps or longer were observed in both MD simulations (Table 2). The largest unfolding of 26 ps was found in the α HTH trajectory after 4090 ps when the $\alpha 2$ C-end became predominantly unfolded. The unfolded α HTH $\alpha 2$ C-end formed a cavity where a water molecule was internalized several times around 4500 and 4800 ps (Fig. 1). A water molecule was underneath the peptide surface inside the α -helix core.

Comparison of previously published RMSD and RMSF values for each residue in the β PTH [25] and α HTH [26] MD trajectories revealed substantial similarity in patterns for RMSD of all heavy atoms and RMSF values for these peptides (Fig. 2). Because the simulation boxes contained 9 and 10 Cl^- anions for β PTH and α HTH, respectively, RMSD and RMSF values reflected intrinsic dynamics of the peptides in water and interactions with Cl^- anions. The highest RMSD values for all heavy atoms in both peptides were found for R17 and R19 which belong to the L1 loop. β PTH displayed larger RMSD values for the backbone atoms in the L1 and L2 loops as compared to α HTH. An increase of RMSD in the β PTH L2 loop can be explained by interactions of L37 with water while α HTH contains glycine at position 37. However, large differences in the backbone RMSD values in the L1 loop cannot be explained by the local differences in the primary sequence. The all heavy atom RMSD values for residues of the R30 hydrogen bonding network were considerably higher for β PTH than for α HTH as well.

The β PTH RMSF values also were mainly higher or equal to that of α HTH (Fig. 2C). The largest fluctuation motions were observed in the L1 loop with the flanking N-end of the $\alpha 2$ -helix and the L2 loop in both peptides. The main differences in RMSF values were observed in both loops, the $\alpha 2$ N-end, and the α HTH R30 network. Interestingly, the RMSF values for the $\alpha 2$ C-end where a water molecule was found were relatively low and identical for α HTH and β PTH except at position 27 containing glycine and asparagine residues, respectively. The RMSF values were almost identical for K1, R19, and the $\alpha 1$ N-end in addition to several cysteine residues forming disulfide bonds. K1 and R10 in the $\alpha 1$ N-end belong to the phospholipid-binding site. However, the role of R19 which is located in the middle of the L1 loop is not clear.

To determine if structural changes within the peptide or interactions with water induced unfolding, time-dependent relations between selected hydrogen bonds, dihedral backbone angles, SAA for backbone atoms (SAA_{bb}) and unfolding were statistically analyzed in the β PTH and α HTH MD trajectories (Table 1). The selected characteristics were compared within 2 ps before each unfolding event except when the $\alpha 2$ C-end was in the predominantly unfolded state.

The statistical analysis indicated that the entire $\alpha 2$ helix and the $\alpha 1$ C-end undergo structural modulations within 2 ps before unfolding (Table 2). A correlation with unfolding was found for residues of the $\alpha 2$ C-end, in particular, for SAA_{bb} values of N(G)27, A26, and C29 and the hydrogen bond A26-O:C31N as expected. These changes reflected α -helix/coil transition. Unexpectedly, a correlation was found for residues of the $\alpha 2$ N-end that included the SAA_{bb} values for K23 and L24 and the hydrogen bond Q22-O:A26-N. Furthermore,

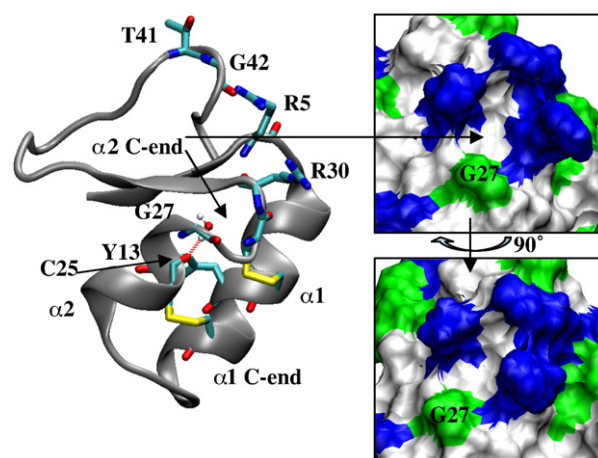


Fig. 1. An internalized water molecule inside the unfolded $\alpha 2$ C-end of α HTH. The water molecule is hydrogen-bonded to C25-O. Residues of the R30 hydrogen bonding network with C25 are shown as licorice and water as stick-and-ball representations. Inserts show the peptide surface at the $\alpha 2$ C-end.

SAA_{bb} of the $\alpha 1$ C-end residues L15 and R17 that are found on the other end of the α -helix core, also correlated with unfolding. Another remote residue which was associated with unfolding, K1, does not belong to the α -helix core. K1 together with R17 belong to the

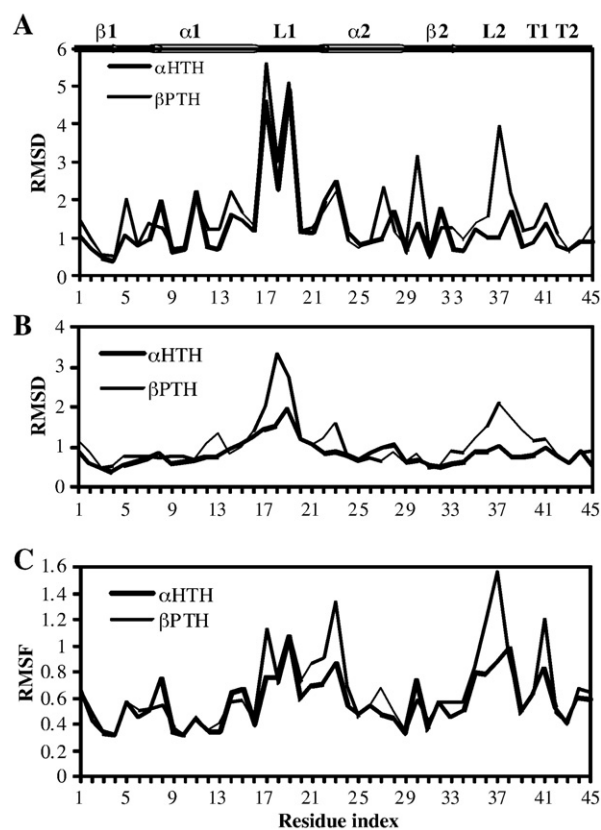


Fig. 2. Comparison of RMSD and RMSF of β PTH (continuous line) and α HTH (heavy continuous line) as functions of residue indices (in Å). (A) RMSD for all heavy atoms and (B) RMSD for the backbone atoms between the MD and the initial structures, and (C) RMSF for the MD trajectories with Cl^- anions in explicit water at 300 K. The average values were calculated over the last ns for β PTH and the last two ns for α HTH. Schematic representation of the secondary structure for the crystal structure of β PTH is shown above the plot in correspondence with residue indices. The data for β PTH are from Oard et al., 2006, Fig. 4 (line – no metal ions), and the data for α HTH are from Oard et al., 2007, Fig. 4 (line – no ions).

Table 2
Characteristics of α HTH and β PTH significantly changing within 2 ps before unfolding of the $\alpha 2$ C-end.

Characteristics	β PTH	α HTH	Localization
Number of unfolding events	21	62 ^a	$\alpha 2$ C-end
Hydrogen bonds	Q22-O:A26-N, A26-O:C31-N	Q22-O:A26-N, A26-O:C31-N	$\alpha 2$ C-end
Dihedral backbone angles (ψ)	N27	G27	$\alpha 2$ C-end
SAA _{bb} ^b	–	K1	B-sheet
	L15, R17	L15, R17	$\alpha 1$ C-end
	L24	K23, L24	$\alpha 2$ N-end
	A26, N27, C29	A26, G27, C29	$\alpha 2$ C-end

^a The unfolding events after the $\alpha 2$ C-end became predominantly unfolded are excluded.

^b Solvent assessable area of the backbone atoms.

phospholipid-binding site. Results for β PTH and α HTH were very similar with only two exceptions. Correlations of unfolding to SAAbb of K1 or K23 were not found in β PTH.

Among tested dihedral backbone angles, only the ψ dihedral angle of N27 in β PTH and G27 in α HTH which belong to both the R30 network and the α 2 C-end correlated with unfolding. No correlations within preceding 2 ps were found for other residues of the R30 regulating network including the R30-O;R5-NE and the G27-O;R30-N hydrogen bonds. However, association between these hydrogen bonds and unfolding of the α 2 C-end was shown previously in both peptides [25,26]. These results suggested that analysis of a larger time interval before unfolding was necessary to show correlation with these hydrogen bonds as well as associations preceding and affecting these hydrogen bonds.

3.2. Anions induced unfolding of the C-end of the α HTH α 2-helix

Further analysis was performed for eight series of the α 2 C-end unfolding events which were found in the α HTH MD simulation that allowed to increase a preceding time interval to 100 ps. Table 3, Column 1 lists all eight independent series which were found in the α HTH MD simulation between 2 and 5 ns. The series ranged from 2 to 150 ps and were separated by at least 110 ps between each other. The time evolution of the G27 and V28 φ and ψ dihedral angles along with the secondary structure were used to determine α 2 C-end unfolding events (Fig. S2, S3). More than 300 characteristics were analyzed within a 100 ps interval before each series to investigate associations of the α 2 C-end unfolding with structural changes within the peptide as well as interactions with water and Cl^- anions. Time evolution of torsion angles, ion interaction energy (E_{ion}), distances, and SAA for representative residues is shown in Figures S3, 3, S4, and S5, respectively, and results are summarized in Table 3.

Table 3, Column 2 shows the backbone dihedral angles of the α 2 C-end residues which were perturbed during the unfolding series. Columns 3 and 4 list residues whose torsion angles became perturbed at the beginning and within 100 ps before a series of unfolding, correspondently. The last two columns contain residues with significant shift in E_{ion} within the same time intervals.

Table 3 demonstrates that each series of the α 2 C-end unfolding was associated with conformational perturbations in the R30 hydrogen bonding network. The torsion angles of R30 and/or R5, which constitute the center of the R30 network, were perturbed within 100 ps before each series. Seven out of eight series were preceded by conformational perturbations in the α 1 C-end, in particular, residues L15, C16, and/or R17. This is consistent with

results of the statistical analysis indicating correlation with SAAbb of L15 and R17. Similarly, an association was found for K1. The major affected characteristic for K1 was E_{ion} between K1 and Cl^- anions. A considerable shift in the K1 E_{ion} was found before six series of the α 2 C-end unfolding (Fig. 3).

Furthermore, each series of the α 2 C-end unfolding was associated with interactions of Cl^- anions with residues of the R30 network G42-R5-R30-G27 and/or the phospholipid-binding site which includes K1, S2, R10, Y13, R17, and Q22 (Table 3). One of the largest series of the α 2 C-end unfolding occurred between 3320 and 3480 ps (Figs. S3A, S2B) during a strong interaction of anions with the central residues of the R30 hydrogen bonding network, R5 and R30 (Fig. 3). The longest unfolding event of this series coincided with the largest R30 E_{ion} values around 3410 ps. These interactions caused considerable perturbations in R5 φ and R30 ψ backbone dihedral angles which persisted beyond interactions with anions. At 2300, 2850, 3640, and 3750 ps, anions simultaneously interacted with the phospholipid-binding site and the peripheral residues of the R30 network, in particular, G42 and neighboring T41 and P40. The subsequent rotation of the T41 side chain around the χ 1 torsion angle (Fig. S3A) brought the T41 hydroxyl group to G42-N. The latter passed the perturbation down the R30 network as evidenced by perturbations in the R30, R5, G27, and V28 torsion angles causing a series of the α 2 C-end unfolding.

The 3060, 3950, and 4090-ps series were caused by interactions of anions with the phospholipid-binding site during conformational perturbations in the R30 network. For the 3060-ps series, an anion became trapped between N11 and N14 from 2850 to 3000 ps attracting R19 to the α 1 C-end. The R19 guanido group approached the hydrophobic area between the α 2 N-end and α 1 C-end pushing away the L15 and K23 side chains (Fig. S3). The K23 side chain rotated toward the K32 side chain, and the later rotated toward R5. Perturbation of the R5 χ 2 was passed to other residues of the R30 network. During these conformational perturbations, E_{ion} values for K1 and R17 started to shift, and the α 2 C-end unfolded. The 3950-ps unfolding series started upon interactions of anions with K1, R17, R19, and Q22 during the constraint in the R30 backbone which started around 3900 ps after a considerable shift in the E_{ion} of R17 and Q22. Conformations of L15, C16, R17, R19, and Q22 on one end of the α -helical core and R5, R30, K32, and T41 on the opposite end became perturbed before this unfolding series.

The largest unfolding series that started at 4090 ps was caused by interactions of anions with the phospholipid-binding site, while the R5 side chain was rotated to G42. This switch in the R30 network was shown by us previously to cause instability in the α 2 C-end [25,26].

Table 3
Characteristics of α HTH significantly changing within 100 ps before the series of unfolding of the α 2 C-end.

Unfolding of the α 2 C-end		Residues with perturbed backbone (φ , ψ) and side-chain torsion angles (χ 1, χ 2)		Residues with shift in ion interaction energy (E_{ion})	
Time (ps)	Perturbed torsion angles	At the beginning of unfolding	Within 100 ps before unfolding	At the beginning of unfolding	Within 100 ps before unfolding
2300	G27 φ	R30 $\psi^{\text{a,b}}$, K38 φ , T41 χ 1	N11 χ 2, L15 χ 1, R17 χ 2, K32 φ , K38 φ χ 1	P40, T41	K1, R10, N14, R17 , A21, Q22
2850	G27 φ	N11 χ 2 ψ , R30 χ 1	R30 χ 1, K38 χ 2, T41 χ 1	N11	K1, R10, N14, R17, K38 , T41
3060–3130	G27 φ	R5 χ 2, K23 χ 2	L15 χ 2, R19 φ , K23 χ 2, R30 ψ , K32 φ χ 1		K1, N11, N14, R17 , G37
3320–3480	G27 ψ V28 φ	R30 χ 1	L15 ψ , R30 χ 2, K32 χ 2	Ans1	R5 , N11, N14, R17, R19, R30 , K32
3640	G27 ψ V28 φ	R30 ψ	R5 φ , N11 χ 2, R17 χ 2, R30 ψ , K32 χ 1, K38 ψ χ 1, K45 χ 2	K1, P40 , T41 , P44	K1, R5 , R10, R17 , V18, K38 , T41 , Gly42 , P44
3750	V28 φ	R5 φ , T41 χ 1, K45 χ 2	K1 χ 2, R5 φ , L15 φ , K23 ψ , R30 ψ , K38 ψ , K45 χ 2	K1, S2, K38, T41 , P44	K1 , R10, N11, G37, K38 , P40, T41 , Gly42 , P44, K45
3950	G27 ψ V28 φ	N11 χ 2, R17 χ 2	R5 φ , L15 ψ , C16 φ , R17 χ 2, R19 χ 1, Q22 χ 1, R30 ψ , K32 φ χ 1, T41 χ 1	K1	K1 , R17 , R19 , Q22
4090–5000	G27 φ ψ V28 φ ψ	R5 χ 2, T41 χ 1	K1 χ 1, N11 χ 2, C16 φ , R17 χ 2, R19 ψ , K23 ψ , K38 φ , T41 χ 1	N11, R17, Q22, K23	N11 , R17 , Q22 , K23 , K32

^a Residues with changes in torsion angles directly related to changes of E_{ion} are shown in bold.

^b Residues of the R30 network are underlined, and residues of the phospholipid-binding site are shown in italics.

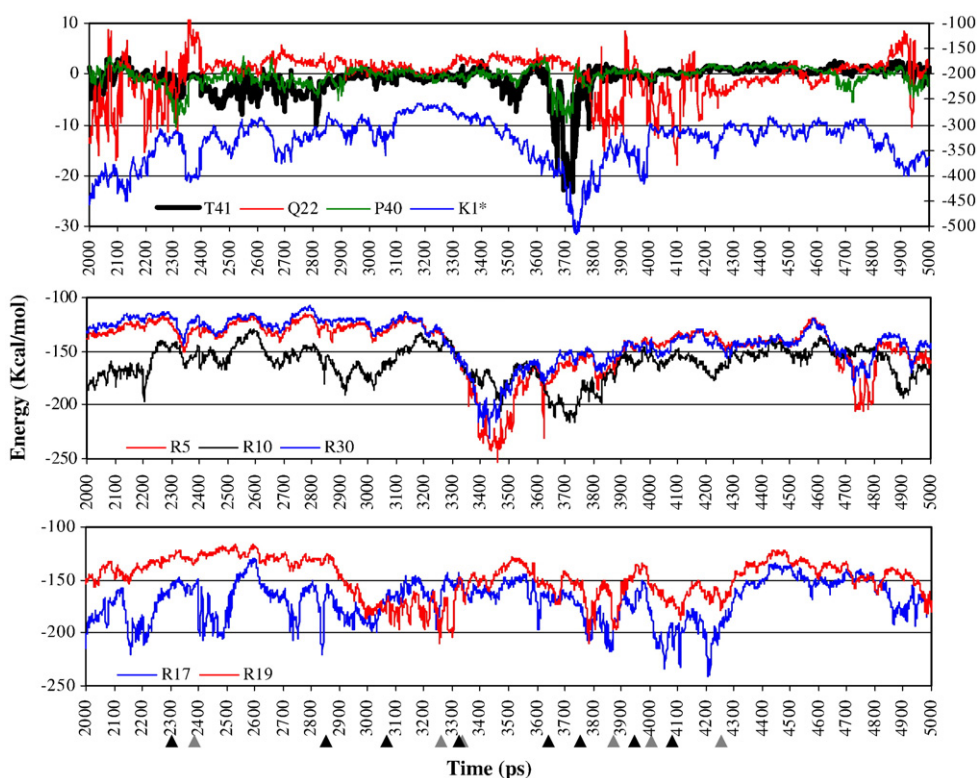


Fig. 3. Time evolution of ion interaction energies (E_{ion}) (in Kcal/mol) for selected residues with Cl^- anions between 2 and 5 ns. Black and gray arrows mark times of unfolding of the $\alpha 2$ C-end and the $\alpha 1$ C-end, correspondently. *Values are shown on the secondary axis.

The 3950-ps unfolding series, which was accompanied by the described above constraint in the R30 backbone, induced a considerable perturbation of the R30 side chain. Rotation of the latter was followed by the rotation of the R5 side chain away and toward G42 (see distance between Gly42-O and R5-NH1, Fig. S4B). A strong hydrogen bond R5-NH1:G42-O was formed around 4000 ps indicating a switch in the R30 network. The E_{ion} for R17, Q22, and K23 started to shift at 4050 ps resulting in destabilization of the $\alpha 2$ C-end.

All series of the $\alpha 2$ C-end unfolding were initiated upon: i) strong interactions of anions with the central residues of the R30 network, ii) simultaneous interactions of anions with residues of the R30 network and phospholipid-binding site, and iii) interactions of anion with the phospholipid-binding site during considerable perturbations in the R30 network.

3.3. Anions triggered unfolding of the C-end of the αHTH $\alpha 1$ helix

Dynamic modulations similar to the $\alpha 2$ C-end unfolding, although less frequent, were also found at the $\alpha 1$ C-end. Unfolding of the $\alpha 1$ C-end was identified by perturbations of the φ and ψ backbone dihedral angles (φ, ψ) of the $\alpha 1$ C-end residues L15 and C16 (Fig. S3B) and α -helix/coil transition of the secondary structure (Fig. S2). L15 existed in the ($-90^\circ, -45^\circ$) and ($-70^\circ, -45^\circ$) conformations, and C16 maintained primarily the ($-70^\circ, -55^\circ$) conformation. When the $\alpha 1$ C-end unfolded, the L15 ψ and C16 φ dihedral angles switched to assume the 0° and -110° values, respectively. Six series of the $\alpha 1$ C-end unfolding were found in the αHTH simulation between 2 and 5 ns ranging from 2 to 70 ps (Table 4, Column 1). To investigate a series of the $\alpha 1$ C-end unfolding, time evolution of backbone and side-chain dihedral angles (Fig. S3) and E_{ion} with Cl^- ions (Fig. 3) for all residues was analyzed within 100 ps before each series. Table 4 demonstrates that all series for the $\alpha 1$ C-end were induced by Cl^- anions similar to that for the $\alpha 2$ C-end. In addition, each series of the $\alpha 1$ C-end unfolding was preceded by a $\alpha 2$ C-end unfolding series.

Interactions of Cl^- anions with residues of the phospholipid-binding site preceded each series of the $\alpha 1$ C-end unfolding. A considerable shift of the E_{ion} value for R17 combined with that for K1, Q22, or R19 was observed within 100 ps before each unfolding series. K1, R17, and Q22 belong to the phospholipid-binding site. R17, R19, and Q22 are located in the L1 loop with R17 flanking the $\alpha 1$ C-end. Perturbations in the side chains and/or backbone torsion angles of these residues were transferred to C16 and L15. For example, the E_{ion} values for Q22 and then R17 shifted before the 2390-ps series of unfolding. The R17 side chain became perturbed, and R19, which is located between R17 and Q22, rotated around the χ_2 angle from 180° to -60° (Fig. S3B). The R19 guanido group came within 3 \AA of the L15-O backbone (Fig. S4C) perturbing the L15 ψ dihedral angle. Small perturbation of the C16 φ , observed during interactions of ions with R17 and Q22, peaked as well when the R19 side chain rotated.

Each $\alpha 1$ C-end unfolding series was preceded by a $\alpha 2$ C-end unfolding series from 60 to 130 ps. For example, strong interactions of anions with R17 and Q22 were observed within 100 ps before 2200 and 2390 ps. However, the unfolding series was triggered only at 2390 ps. The difference between 2200 and 2390 ps was unfolding of the $\alpha 2$ C-end which occurred shortly before 2390 ps. Each large series of the $\alpha 1$ C-end unfolding was preceded by a large series of the $\alpha 2$ C-end unfolding. The 3330-ps series of the $\alpha 1$ C-end unfolding started shortly after the beginning of the large 3320-ps series of the $\alpha 2$ C-end unfolding. Both the $\alpha 2$ C-end and the $\alpha 1$ C-end became perturbed for more than 100 ps upon simultaneous strong interactions of anions with R5 and R30 on one end and R17 with R19 on another end of the α -helix core (Tables 3 and 4). The $\alpha 1$ C-end was destabilized at 4260 ps after the $\alpha 2$ C-end became predominantly unfolded.

Each large series of the $\alpha 1$ C-end unfolding, in particular, the 3330-, 4010-, and 4260-ps series, included extension modulations which alternated with unfolding events. These series can be characterized as alternating unfolding/extension modulation at the $\alpha 1$ C-end. Fig. S2B illustrates the 3330-ps series of alternating unfolding/extension during

Table 4
Characteristics of α HTH significantly changing within 100 ps before the series of unfolding of the α 1 C-end.

Unfolding of the α 1 C-end		Residues with perturbed backbone (φ, ψ) and side-chain torsion angles (χ_1, χ_2)		Residues with shift of ion interaction energy (E_{ion})	
Time (ps)	Perturbed torsion angles	At the beginning of unfolding	Within 100 ps before unfolding	At the beginning of unfolding	Within 100 ps before unfolding
2390	C16 φ L15 ψ	K1 χ_1^a , L15 χ_1^b , R19 χ_2	R5 φ , R17 χ_2 , G27 φ , R30 ψ , K38 φ ψ R19 φ , G27 φ , K38 ψ χ_2	K1 , R17 , L33, T34	K1, Q22, K32, S35, P40, T41
3250	C16 φ L15 ψ				N11, N14, R17, R19
3330–3400	C16 φ L15 ψ	R17 ψ , R19 φ , V28 φ , R30 χ_1	G27 ψ , R30 χ_2 , K32 χ_2	N11, N14	R5 , N11, N14, R17 , R19 , V28 , R30 , R32
3880	C16 φ L15 ψ	R17 ψ χ_2 , R19 χ_1 , Q22 χ_1	R5 φ , N11 χ_2 , R17 χ_2 , R19 φ , Q22 χ_1 , G27 φ , V28 φ , K32 χ_1 χ_2 , K45 χ_2 R5 φ χ_2 , N11 χ_2 , L15 φ , R17 χ_2 , K23 ψ , G27 ψ , V28 φ , R30 ψ χ_1 , T41 χ_1	Y13, R17 , R19	K1, S2, R10, L15, R17 , R19 , Q22 , K32
4010–4060	C16 φ	K1 χ_1 ψ , R17 χ_2	K1 χ_1 , R5 χ_1 χ_2 , N11 χ_2 , R17 χ_2 ψ , R19 χ_1 φ , Q22 χ_1 , R30 χ_2 , K32 χ_1 ψ , K38 φ	N11, Q22	K1 , R17 , R19, Q22
4260–5000	C16 φ L15 ψ	R19 χ_1 , Q22 χ_2 , V28 ψ φ , K38 φ , K45 χ_2		K23	K1 , R17 , K23, K45

^{a, b} Same as for Table 3.

strong interactions of anions with R5 and R30. Similar modulations were observed at 4010–ps after the conformational switch in the R30 regulating network and after the α 2 C-end became predominantly unfolded. In particular, unfolding/extension modulations occurred around 4500 and 4800 ps when the R19 guanido group approached the α 1 C-end (see distance L15–O R19–NE, Fig. S4; Fig. S2C). An internalized water molecule was found in the unfolded α 2 C-end at that time.

Thus, all α 1 C-end unfolding series were triggered by Cl^- anions. Simultaneous increases of E_{ion} for the residues of the phospholipid-binding site R17, K1, and Q22 or R17 with R19 were observed within 100 ps before each unfolding series. Unfolding of the α 1 C-end was observed only when interactions with anions were preceded by unfolding of the α 2 C-end. These results together with statistical analysis described in the Section 1 point to an association between unfolding of the α 1 C-end and the α 2 C-end.

3.4. Zones of anion concentration

Previously we analyzed the anion distribution map for the α HTH MD trajectory [26]. Here we report on zones of Cl^- anion concentration at the peptide surface as potential regions for interactions with negatively charged head groups of phospholipids. Cl^- ions predominantly traced the phospholipid-binding site and the R30 hydrogen binding network, which are located at the inner and the outer corner of the thionin global Γ fold, respectively (Fig. 4). The major zones of anion concentration were at the phospholipid-binding site.

Cl^- anions interacted with the residues of the phospholipid-binding site numerous times during the MD simulation (Figs. 3 and 4A). Anions were observed most often at the K1 side chain or the N-terminus sometimes only 3 Å away (Fig. 4A, the Cl^- anion colored in gray) inducing large shifts of the K1 E_{ion} , the largest E_{ion} values in the peptide. Another “hot” zone was the R17 guanido group which trapped Cl^- anions several times for more than 100 ps. Considerable interactions of Cl^- anions were observed with the R10, K45, and Q22 side chains. Anions traced the phospholipid-binding site sometimes two to three at a time migrating between the side chains of K45, K1, R10, R17, Y13, S2, and Q22. One anion persisted between Y13–OH, Q22–NE, and R17–NH1 4.3, 3.5, and 4.1 Å away, respectively, for nearly 50 ps.

The entire arm surface and the outer corner of the Γ were accessible to anions. Two zones of anion concentration were observed at the outer corner of the Γ (Fig. 4B). Strong interactions were observed with the center of the R30 regulating network where Cl^- anions persisted in

front of R5 from 3300 to 3500 ps and from 4700 to 4800 ps at times only 2.3 Å away from the R5 guanido group (Fig. 4B, the Cl^- ion colored in gray). Cl^- ions frequently circulated around the peripheral residue of the R30 network, G42 and especially its neighbor T41 located at the ridge of the peptide arm. Most often an anion shifted toward the K38 side chain or moved to the opposite site and fluctuated in a triangle of the T41, R5, and K32 side chains approximately 3.9 Å from G42–N.

In contrast to the arm and both corners of the Γ fold, the stem surface was mainly inaccessible to anions. A Cl^- anion persisted between the N11 and N14 side chains twice for more than 100 ps during the MD trajectory at ~2900 and 3400 ps. Unexpectedly, anions were found two times in the middle of the α 1/ α 2 hydrophobic region, interacting with the backbone atoms of the α 1 C-end (Fig. 4B). An anion was observed between the R19 side chain, L15–O, and C16–N at ~3300 and 3800 ps. The backbone nitrogen atom of the highly conserved residue C16 was the closest to an anion in both cases. At 3300 ps, another anion strongly interacted with the center of the R30 network generating the largest E_{ion} values for R5 and R30. At 3800 ps, two anions simultaneously interacted with the phospholipid-binding

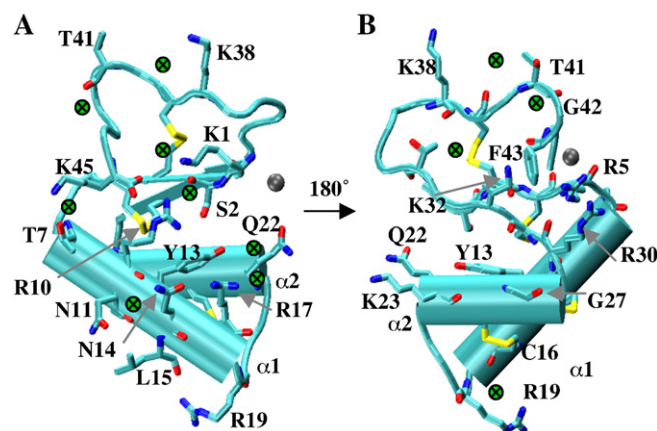


Fig. 4. Zones of Cl^- anion concentration on the α HTH surface (A) at the phospholipid-binding site and the inner corner of the Γ fold and (B) the R30 regulating network at the outer corner of the Γ fold and the middle of the α 1/ α 2 hydrophobic region. Green circles represent zones of anion concentration observed between 2 and 5 ns of the MD simulation. Snapshots of secondary structure are shown for (A) 2370 and (B) 3380 ps, respectively, and Cl^- anions which belong to a particular snapshot are colored in gray.

site and the peripheral residues of the R30 network. Both events were preceded by the series of the $\alpha 2$ C-end unfolding which was followed by the $\alpha 1$ C-end unfolding. Therefore, the $\alpha 1/\alpha 2$ hydrophobic region became accessible to anions during strong interactions of anions either with the R30 network or the phospholipid-binding site and the R30 network which were accompanied by large conformational perturbations in the α -helix core. Anions were found in the middle of the $\alpha 1/\alpha 2$ hydrophobic region between the unfolded $\alpha 1$ C-end and the R19 side chain.

3.5. Anions triggered rearrangements in α HTH

Two multi-residue rearrangements were observed during the MD simulation between 3600 and 3800 ps and from 4000 to 4260 ps. The former was triggered by concurrent strong interactions of anions with the phospholipid-binding site and the R30 regulating network. The latter was the result of strong interactions of anions with the phospholipid-binding site during conformational perturbations in the R30 network.

Two to three anions interacted with residues of the phospholipid-binding site and an anion with the R30 regulating network between 3600 and 3800 ps. The E_{ion} values shifted for several residues of the R30 regulating network (R5, T41, and G42) and the phospholipid-binding site (K1, S2, R10, and R17) (Fig. 3). Anions persisted between T41, R5, and K32 on one side and between Y13, Q22, and R17 on another side (see Section 4). Attracted by an anion, the K32 amino group rotated and became exposed to the R5 guanido group contributing to a constraint in the R5 and R30 backbones. Accompanied by conformational changes in R17, K23, and the $\alpha 2$ C-end, the C-terminal residue K45 became considerably perturbed (Fig. S3). The latter forms three out of five

hydrogen bonds of the global Γ fold. The K38 side chain rotated toward K1, pushing it away and causing a long-lasting constraint in the K38 backbone. At the end of these perturbations, the Q22 χ_1 switched from 60° to -60° that brought the Q22-OE1 within 3 \AA from Y13-OH (Fig. 5B and D). Because Q22 is located at the $\alpha 2$ N-end, this rotation linked the $\alpha 2$ N-end with the center of the phospholipid-binding site.

Rotation of the R5 χ_2 from -180° to -60° , which was induced by anions as described in Section 2, initiated the 4000-ps rearrangement (Fig. S3). This rotation started large perturbations in the R30 network that culminated at 4090 ps causing the $\alpha 2$ C-end to unfold. Predominantly two anions simultaneously interacted with the phospholipid-binding site between 4000 and 4260 ps. One anion persisted between Q22 and K23 and another moved around the R17 guanido group. Following the unfolding, the K45 side chain rotated similarly to that observed during the 3600-ps rearrangement. Conformations of K1, R17, Q22, K23, K32, and K38 also became considerably perturbed as during the first rearrangement. Almost immediately after rotation of the K45 side chain, the R30 χ_1 rotamer assumed a highly probable conformation with the (φ, ψ, χ_1) values at ($55^\circ, 60^\circ, -60^\circ$) unlike before when zero probability conformations with ($55^\circ, 0^\circ, -60^\circ$) and ($55^\circ, 0^\circ, 180^\circ$) values were frequently observed (Fig. S3). The R5 side chain rotated further to complete the conformational switch in the R30 network by establishing a hydrogen bond G42-O:R5-NE (Fig. 5A and C). After the conformational switch, the R19 χ_1 rotamer ($-120^\circ, 0^\circ, -170^\circ$) became predominant positioning the R19 guanido group in front of the $\alpha 1/\alpha 2$ hydrophobic region, in particular, between the $\alpha 1$ C-end and the $\alpha 2$ N-end on the far end of the predominantly hydrophobic stem (Fig. 5). After the 4000-ps rearrangement, the $\alpha 2$ C-end became predominantly unfolded, and the $\alpha 1$ C-end was destabilized.

Analysis of interaction energies between selected pairs of residues (E_{res}) which participated in both rearrangements revealed auxiliary residues of the phospholipid-binding site and the R30 network (Fig. 6).

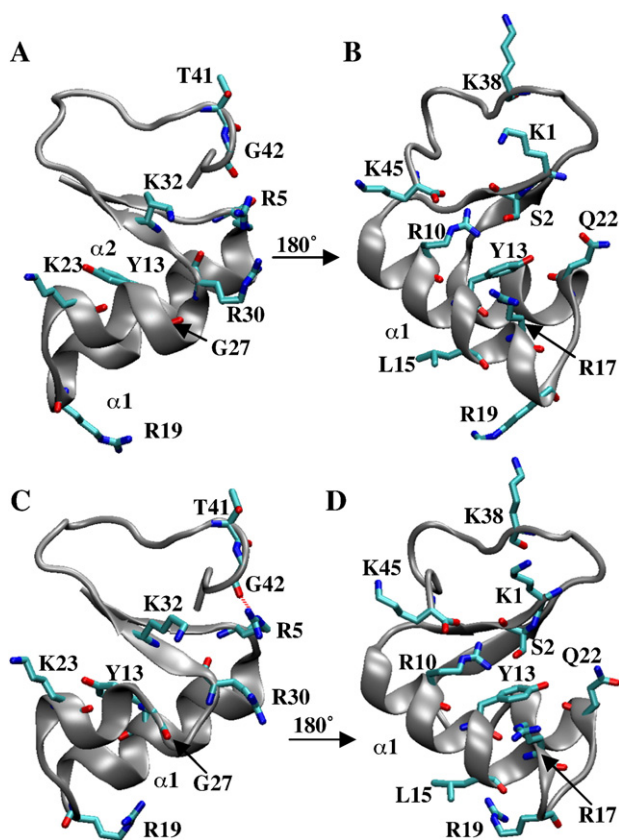


Fig. 5. Conformational changes in α HTH after the 3600-ps and 4000-ps rearrangements. Representative structures (A, B) before 3600 ps and (C, D) after 4260 ps are shown (A, C) at the outer corner and (B, D) the inner corner of the Γ fold. Residues of the R30 network, the phospholipid-binding site, and the auxiliary residues are shown as licorice.

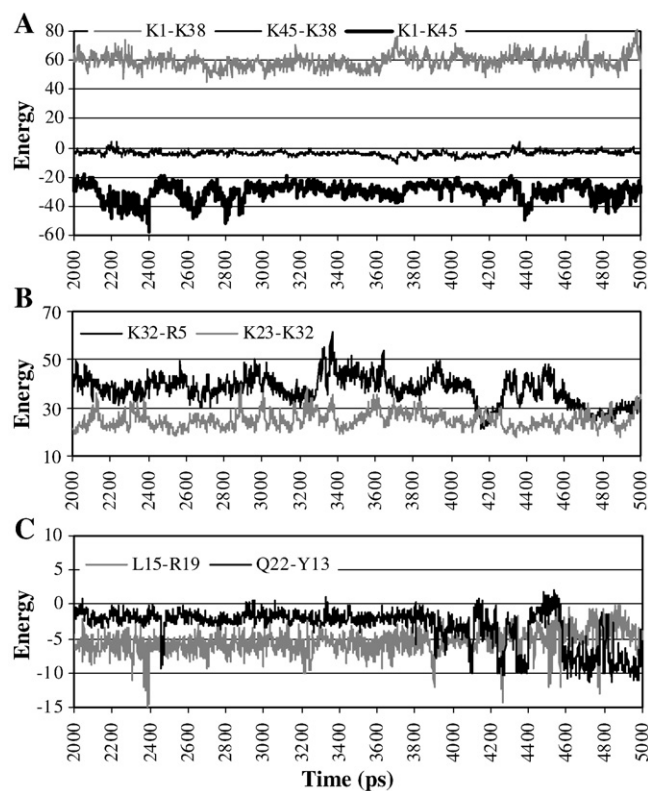


Fig. 6. Time evolution of residue interaction energies (E_{res}) (in Kcal/mol) between the selected residues and the residues of the phospholipid-binding site, the R30 network and at the C-end of the $\alpha 1$ helix between 2 and 5 ns.

The residue of the phospholipid-binding site K1 positively interacted with the C-terminal residue K45 while negatively with K38. Large attractive E_{res} values between K1 and K45 indicated a direct link of the phospholipid-binding site with K45. Strong repulsive interactions between K1 and K38 during the entire simulation and particularly around 3700 ps explained concurrent rotations of the K1 and K38 side chains. Attractive interactions between Y13, which is the central residues of the phospholipid-binding site, and Q22 considerably increased after the Q22 side chain rotated toward Y13 during the 3600-ps rearrangement. Interestingly, the K32 conformation was considerably perturbed before both rotations of the K45 side chain during rearrangements and before the 3060, 3320, and 3950-ps $\alpha 2$ C-end unfolding series (Fig. S3). Analysis of E_{res} showed that K32 interacted repulsively with R30 and especially with R5 on one side and with K23 at the $\alpha 2$ N-end on another side. Perturbations in K32, which was otherwise hidden behind F43, exposed the K32 side chain to R5 increasing repulsive interactions and promoting perturbations in the R30 network. Although K32 interacted weaker with K23 than with R5, the E_{res} values between K32 and K23 exceeded 30 Kcal/mol several times during the MD simulation. Thus, analysis of residue interaction energies showed that the phospholipid-binding site in α HTH strongly interacts with K45 and K38, and Q22 can link the site's center with the $\alpha 2$ N-end. The central residues of the R30 network can strongly interact with K32 which links the R30 network also with the $\alpha 2$ N-end through K23. This could explain the 4000-ps rearrangement which progressed during interactions of anions with Q22, K23, and R17 while the Q22 side chain was within a hydrogen bonding distance to Y13.

4. Discussion

The presence of electrostatic interactions between thionins, these extremely positively charged peptides, and negatively charged head-groups of membrane phospholipids was documented experimentally [5,19]. In this study analysis of the MD simulations provides new insights on electrostatic interactions between thionins and negatively charged ions. We have demonstrated that anions induced conformational changes in the α HTH antiparallel double α -helix core. Anions induced unfolding not only of the $\alpha 2$ C-end, but also of the C-end of the $\alpha 1$ -helix which are located on the opposite ends of the α -helix core. These anion-induced structural changes led to penetration of a water molecule inside the unfolded $\alpha 2$ C-end. Furthermore, analysis of the MD trajectory pointed to localization of anion attracting zones on the peptide surfaces as well as auxiliary residues of the phospholipid-binding site and the R30 regulating network.

We previously reported that the $\alpha 2$ C-end was intrinsically dynamic and periodically unfolded in both β PTH and α HTH [25,26]. However, reasons of these dynamic modulations were not understood. The present study revealed a critical relation between unfolding of the $\alpha 2$ C-end and interactions of anions with the R30 hydrogen bonding network and the phospholipid-binding site. Interaction of an anion with the central residues of the R30 network, R5 and R30, was sufficient to trigger unfolding. Interactions of anions with the phospholipid-binding site triggered unfolding only when another anion simultaneously interacted with the peripheral residues of the R30 network or during considerable structural perturbations in the R30 network. The R30 regulating network was involved in unfolding of the $\alpha 2$ C-end in β PTH and α HTH in the presence of cations [25,26]. Those MD trajectories with cations contained also anions. The trajectories analyzed in this work contained only anions. Combined together, our results suggest that the R30 network creates an anion-inducible spring that opens an entrance into the α -helix core.

All unfolding events observed for the $\alpha 1$ C-end were also induced by interactions with anions. We found two necessary conditions required for unfolding of the $\alpha 1$ C-end: (i) simultaneous interactions of anions with at least two residues of the phospholipid-binding site (K1, R17, and Q22) or with R17 and R19 and (ii) a preceding unfolding

of the $\alpha 2$ C-end. R17 flanks the $\alpha 1$ C-end, and the R19 guanido group can reach backbone atoms of the located in the $\alpha 1$ C-end L15. Perturbations of these residues can affect the $\alpha 1$ C-end. However, dependence of unfolding of the $\alpha 1$ C-end on a preceding unfolding of the $\alpha 2$ C-end is not self-evident. Nevertheless, an association between unfolding of the $\alpha 2$ C-end and the $\alpha 1$ C-end was shown by two methods in this study including the statistical analysis. Our statistical analysis revealed a correlation between unfolding of the $\alpha 2$ C-end and SAA of backbone atoms of L15 with R17 in α HTH and β PTH indicating structural changes in the $\alpha 1$ C-end upon unfolding of the $\alpha 2$ C-end.

The crystallographic data support existence of the $\alpha 1$ C-end in the folded and unfolded states. In the β -hordothionin crystal structure (PDB ID: 1WUW), one monomer has the folded $\alpha 1$ C-end while the $\alpha 1$ C-end of the other monomer is unfolded [46]. The R30 regulating network and the phospholipid-binding site of both monomers interact with anions, oxygen atoms of the sulfonate and the serine moieties, respectively. However, distances between the residues of the phospholipid-binding site and the serine moiety are shorter for the monomer with the unfolded $\alpha 1$ C-end as compared to that of the monomer with the folded $\alpha 1$ C-end. The shorter distances to the anion incur larger E_{ion} values for the residues of the phospholipid-binding site that is consistent with our findings.

The evidence presented indicates that anions can trigger conformational changes on the opposite ends of the α -helix core that result in penetration of a water molecule inside the unfolded C-end of the $\alpha 2$ helix. These data concur with experimental results indicating an important role of the α -helix core in membrane permeabilization activity. The α -helix core constituted a minimal motif retaining antimicrobial activity as determined by testing several truncated PpTH peptide derivatives [21]. Interestingly, the minimal motif included D32 which is equivalent to R30 in α HTH and β PTH. Stabilization of the α -helix core with the native disulfide bonds was critical for activity. The α -helix core carries 4 out of 6 residues constituting the phospholipid-binding site in $\alpha 1$ -purothionin (R10, Y13, R17, and Q22) [15]. The $\alpha 1$ helix is the most conserved secondary structure within the α -helix core [47]. The L1 loop and the $\alpha 2$ N-end are conserved among hordothionins, purothionins, and avenothionins (type I thionins) while only the residues of the $\alpha 2$ C-end facing outside the α -helical core vary.

Formation of an α -helical bundle as a critical step in membrane-permeabilizing activity was suggested for several amphipathic antimicrobial peptides. The barrel-stave model also known as the helical bundle model has been proposed among others to explain interactions between lytic peptides and membranes (for review see [48]). The model is based on aggregation of α -helices into bundles and insertion into the membrane to form pores. Furthermore, a highly active analog of a lytic peptide magainin, MSI-78, forms an antiparallel dimer to establish a double antiparallel α -helix core, which is found in thionins, when inserted into the membrane [49]. MSI-78 dimers are stabilized by extensive hydrophobic interactions at the interface between two protomers. Inability to form dimers is thought to be responsible for loss of membrane-permeabilizing activity in the inactive magainin analog, MSI-594. The α -helical bundles formed by dimerized amphipathic peptides can also produce ion-selective channels [50–52].

Two-dimensional infrared correlation spectroscopy demonstrated that the thionin α -helical core inserts into the membrane bilayer [5,9]. Formation of cation-selective ion channels in artificial lipid bilayers and in the plasmalemma was shown for β PTH, $\alpha 1$ -purothionin, and $\alpha 2$ -purothionin using electrophysiological measurements [7] and infrared correlation spectroscopy [5,9]. We demonstrated in this work that negatively charged ions, when interacting with the phospholipid-binding site and the R30 regulating network, induce considerable structural perturbations on the opposite ends of the α -helical core. These anion-induced structural changes enable penetration of water inside the α -helical core. Together these findings provide important evidence

toward deciphering a mechanism of membrane-permeabilizing activity by thionins.

Zones of anion concentration found using the MD simulations pointed to potential areas of attraction for negative charges on the α HTH surface. Our MD simulations revealed two new zones of anion attraction in addition to those found in the crystal structures. We found all zones of anion attraction which were observed in the crystal structures that confirms good agreement between results of the MD simulations and crystallographic data. The largest ion interaction energies were observed for K1, and a phosphate ion was found at K1 in the β PTH and α 1-purothionin crystal structures [15,16]. Cl^- ions often persisted around K1-NZ or the N-terminal amino group in locations where anions were found in the crystal structures. Another area of anion concentration in the MD simulations was around the R17 guanido group. Similarly, R17-NE was found bound to the O3 of a glycerol molecule in both β PTH and α 1-purothionin. Moreover, the anion trap between Y13-OH, Q22-NE, and R17-NH1 which was observed in the MD trajectory is very similar to the glycerol-binding site found in the α 1-purothionin crystals that included Y13-OH, Q22-OE, and R17-NE. Similarly, anions were found at the R30 network in the α 1-purothionin and β -hordothionin crystal structures. Dimers in the β PTH and α 1-purothionin crystal structures were anchored by the N11 and N14 side chains that is consistent with the anion attracting zone between the side chains of N11 and N14 in the α HTH MD simulation. N11 and N14 are conserved in the majority of thionins [47].

In addition, our MD simulations revealed zones of anion attraction that were not detected by crystallography. Surfaces around T41 and G42 were highly attractive to anions in the MD trajectory unlike in crystal structures. T41 and Gly42 are the peripheral residues of the R30 regulating network in α HTH. They are located on the ridge at the outer corner of the global Γ fold. The α 1/ α 2 hydrophobic region was void of interactions with anions in all three crystal structures [15,16] (PDB ID: 1WUW). However, the MD simulations revealed that the α 1/ α 2 hydrophobic region can become attractive to anions during simultaneous interactions of anions with the R30 network and the phospholipid-binding site which are accompanied by unfolding of the α 1 and α 2 C-ends. During these perturbations, an anion moved down the α 1/ α 2 hydrophobic region to the α 1 C-end and approached backbone atoms of the highly conserved C16. Thus, the α 1/ α 2 region, in particular at the α 1 C-end, can change from hydrophobic to hydrophilic upon interactions with anions.

Analysis of the anion-induced rearrangements in α HTH reported here also clarifies relations between residues and points to auxiliary residues of the phospholipid-binding site and the R30 network. Experimental data about participation of Q22 in the phospholipid-binding site were inconsistent. The glycerol-binding site included Q22 in the α 1-purothionin crystals while in the β PTH crystals the glycerol-binding site contained K45 [15,16]. Our MD simulations demonstrated that Q22 can directly interact with the middle of the phospholipid-binding site to form a hydrogen bond with Y13-OH. These data support the glycerol-binding site as found in the α 1-purothionin crystal structure. Indeed, this site where all residues belong to one monomer is more probable because thionins are bound to the membrane bilayer in a monomeric form [3,5,18]. In contrast, K45 in the glycerol-binding site of the β PTH crystal structure belonged to a second monomer.

K1, the residue of the phospholipid-binding site with two amino groups, interacted attractively with the carboxyl group of K45 and repulsively with K38. K1 is highly conserved in thionins while K45 is conserved in thionins with four disulphide bonds that are type I and II thionins [47]. K1 participated in the phosphate-binding site in the β PTH and α 1-purothionin crystals [15,16]. However, the role of K45 was not evident as discussed above. Strong interaction energies of K1 with K45 and K38 were maintained throughout our α HTH MD simulations as well as a tilt of the K1 side chain toward the phospholipid-binding site. This tilt kept the amino groups of the K1 side chain and the N-terminus in close proximity to each other helping to concentrate a positive charge

and generate the largest interaction energies between K1 and anions. A combination of attraction to the K45 carboxyl group and repulsion from K38 could maintain that slant and concentrate a positive charge. Although K38 is not conserved, almost all thionins contain a basic residue at position 38 or 41, and both placements should create strong repulsive interactions pushing the K1 side chain away directing it toward the phospholipid-binding site.

Four auxiliary residues K23, K32, T41, and F43 were revealed for the α HTH R30 network. Perturbations of the K32 side chain directly affected the R30 network. The largest interaction energies between K32 and the central residues of the R30 network R5 and R30 were observed when the K32 side chain was exposed to R5 from behind of the F43 side chain. Interestingly, K32 is conserved in thionins, and only residues with bulky chains such as F, Y, and W are found at position 43 [47]. Side chains of these residues can screen the K32 side chain from R5. Furthermore, analysis of interaction energies suggests that perturbations caused by repulsive interactions can be passed from R5 through K32 to K23 and therefore from the R30 network to the α 2 N-end and vice versa. Thus, the α 2 N-end is linked to the phospholipid-binding site by Q22 and to the R30 network by K23. The Q22/K23 pair is found only in puro- and hordothionins, but all of them preserve this pair of residues that suggests an important functional advantage. It appears that puro- and hordothionins have an auxiliary network R(K)5-K32-K23-Q22-Y13 connecting the R30 network with the phospholipid-binding site. This auxiliary network may eliminate a need for simultaneous interactions of anions with the R30 network and the phospholipid-binding site for the α 2 C-end to unfold. In this case, perturbations caused by binding of a phospholipid to the phospholipid-binding site should be transferred through the auxiliary network to the R30 network triggering unfolding of the α 2 C-end.

Another auxiliary residue T41 directly interacted with the peripheral residue of the R30 network G42. Several thionins carry aspartic acid at position 42 and only a few have glycine as α HTH. D42 in β PTH attracted the K5 side chain to generate a switch in the R30 network and unfolding of the α 2 C-end [25]. In α HTH, T41 may modulate acidity of G42-O to attract R5. Rotation of T41-OH to G42-N upon interactions of T41 with anions and the following perturbations in the R30 network were observed repeatedly in this study. Interactions of T41-OH with G42-N can be explained by a decrease of proton density on the T41 hydroxyl oxygen caused by an anion. T41-OH competes with G42-N for a proton causing electron delocalization to G42-O. A resulting increase in acidity of G42-O helps to attract the R5 guanido group. Thus, interactions with anions should increase ability of the T41/G42 pair to attract R5. In contrast, aspartic acid directly attracts R5 that increases a non-specific response. Indeed, the β PTH R30 network containing aspartic acid at position 42 was more susceptible to cations than that of α HTH [25,26]. Thus, the T41/G42 pair can be attributed to increased specificity toward anion induction of the α 2 C-end unfolding.

5. Conclusions

Several properties of α HTH were revealed in this work. (1) Anions can trigger a series of α 2 C-end unfolding by interacting with the R30 regulating network and the phospholipid-binding site. (2) Anions can induce unfolding of the α 1 C-end as well when interacting with at least two residues of the phospholipid-binding site (K1, R17, and Q22) or with R17 and R19. The α 1 C-end unfolding is preceded by unfolding of the α 2 C-end. (3) Unfolding of the α 2 C-end is associated not only with conformational changes in the residues of the R30 network, but also with structural perturbations at the α 1 C-end and the α 2 N-end. These findings suggest that conformational perturbations in the α 2 C-end are passed to the opposite end of the α -helical core. (4) The phospholipid-binding site has the auxiliary residues K45 and K38 which help to concentrate a positive charge at K1. The R30 network also auxiliary residues including K32 and K23 which can modulate perturbations of

the central residues of the R30 network. All puro- and hordothionins appear to have an auxiliary network R(K)5-K32-K23-Q22-Y13 connecting the centers of the R30 network and the phospholipid-binding site. (5) Our results indicate that the R30 regulating network creates an anion-inducible spring which opens an entrance for water into the α -helical core. Penetration of water inside the unfolded $\alpha 2$ C-end and therefore inside the α -helical core is consistent with properties of α -helical bundles to form ion channels and pores in membranes.

Acknowledgment

We thank Dr. Randall Hall, Dept. of Chemistry, Louisiana State University for helping to select analytical methods for the MD trajectory. We thank also Dr. Peter Butko, Dept. of Pharmaceutical Sciences, University of Maryland at Baltimore for reading the manuscript draft and providing helpful insights. This work was supported by LSU AgCenter Experiment Station. Simulations were performed at LSU's Center for Applied Information Technology and Learning (CAPITAL) and Biological Computation and Visualization Center (BCVC).

Appendix A. Supplementary data

Supplementary data associated with this article can be found, in the online version, at doi:10.1016/j.bpc.2009.12.009.

References

- [1] D. Florack, W. Stiekema, Thionins: properties, possible biological roles and mechanisms of action, *Plant Mol. Biol.* 26 (1994) 25.
- [2] F. García-Olmedo, P. Rodríguez-Palenzuela, C. Hernández-Lucas, F. Ponz, C. Marañón, M. Carmona, J. López-Fando, J. Fernández, P. Carbonero, The thionins: a protein family that includes purothionins, viscoctoxins and crambins, *Oxford Surveys Plant. Mol. Cell. Biol.* 6 (1989) 31.
- [3] B. Stec, O. Markman, U. Rao, G. Heffron, S. Henderson, L.P. Vernon, V. Brumfeld, M.M. Teeter, Proposal for molecular mechanism of thionins deduced from physicochemical studies of plant toxins, *J. Pept. Res.* 64 (2004) 210.
- [4] M. Zasloff, Antimicrobial peptides of multicellular organisms, *Nature* 415 (2002) 389.
- [5] J.-A. Richard, I. Kelly, D. Marion, M. Pezolet, M. Auger, Interaction between β -purothionin and dimyristoylphosphatidylglycerol: A ^{31}P -NMR and infrared spectroscopic study, *Biophys. J.* 83 (2002) 2074.
- [6] L. Carrasco, D. Vazquez, C. Hernández-Lucas, P. Carbonero, F. García-Olmedo, Thionins: plant peptides that modify membrane permeability in cultured mammalian cells, *Eur. J. Biochem.* 116 (1981) 185.
- [7] P. Hughes, E. Dennis, M. Whitecross, D. Llewellyn, P. Gage, The cytotoxic plant protein, β -purothionin, forms ion channels in lipid membranes, *J. Biol. Chem.* 275 (2000) 823.
- [8] T. Niidome, S. Anzai, Effect of amino acid substitution in amphiphilic α -helical peptides on peptide-phospholipid membrane interaction, *J. Pept. Sci.* 5 (1999) 298.
- [9] J. Richard, I. Kelly, D. Marion, M. Auger, M. Pézolet, Structure of beta-purothionin in membranes: a two-dimensional infrared correlation spectroscopy study, *Biochemistry* 44 (2005) 52.
- [10] B. Bechinger, A dynamic view of peptides and proteins in membranes, *Cell. Mol. Life Sci.* 65 (2008) 3028.
- [11] K. Thevissen, F. Terras, W.F. Broekaert, Permeability of fungal membranes by plant defensins inhibits fungal growth, *Appl. Environ. Microbiol.* 63 (1999) 5451.
- [12] S. Oard, M.C. Rush, J.H. Oard, Characterization of antimicrobial peptides against a US strain of the rice pathogen *Rhizoctonia solani*, *J. Appl. Microbiol.* 97 (2004) 169.
- [13] W. Powell, C. Catranis, C. Maynard, Synthetic antimicrobial peptide design, *MPMI* 8 (1995) 792.
- [14] J. Sels, J. Mathys, B. De Coninck, B. Cammue, M. De Bolle, Plant pathogenesis-related (PR) proteins: a focus on PR peptides, *Plant Physiol. Biochem.* 46 (2008) 941.
- [15] U. Rao, B. Stec, M. Teeter, Refinement of purothionins reveals solute particles important for lattice formation and toxicity. 1. $\alpha 1$ -purothionin revisited, *Acta Crystallogr., Sect. D* 51 (1995) 904.
- [16] B. Stec, U. Rao, M.M. Teeter, Refinement of purothionins reveals solute particles important for lattice formation and toxicity. Part 2: Structure of beta-purothionin at 1.7 angstroms resolution, *Acta Crystallogr., Sect. D* 51 (1995) 914.
- [17] S. Van Campenhout, L. Sagi, J. Vander Stappen, G. Vlockaert, Characterisation of type-I thionin loci from the A, B, D, and R genomes of wheat and rye, *Theor. Appl. Genet.* 96 (1998) 80.
- [18] J. Caaveiro, A. Molina, P. Rodríguez-Palenzuela, F. Goni, J. Gonzalez-Manas, Interaction of wheat $\{\alpha\}$ -thionin with large unilamellar vesicles, *Protein Sci.* 7 (1998) 2567.
- [19] W. Huang, L.P. Vernon, L.D. Hansen, J.D. Bell, Interactions of thionin from *Pyricularia pubera* with dipalmitoylphosphatidylglycerol large unilamellar vesicles, *Biochemistry* 36 (1997) 2860.
- [20] F. García-Olmedo, A. Molina, J.M. Alamillo, P. Rodríguez-Palenzuela, Plant defense peptides, *Biopolymers* 47 (1998) 479.
- [21] M. Vila-Perello, A. Sanchez-Vallet, F. García-Olmedo, A. Molina, D. Andreu, Structural dissection of a highly knotted peptide reveals minimal motif with antimicrobial activity, *J. Biol. Chem.* 280 (2005) 1661.
- [22] F. Ponz, J. Paz-Ares, C. Hernández-Lucas, F. García-Olmedo, P. Carbonero, Cloning and nucleotide sequence of a cDNA encoding the precursor of the barley toxin alpha-hordothionin, *Eur. J. Biochem.* 156 (1986) 131.
- [23] D.G. Redman, N. Fisher, Purothionin analogues from barley flour, *J. Sci. Food Agric.* 20 (1969) 427.
- [24] F. Ebrahim-Nesbat, S. Bohl, R. Heitefuss, K. Apel, Thionin in cell walls and papillae of barley in compatible and incompatible interactions with *Erysiphe graminis* f. sp. *hordei*, *Physiol. Mol. Plant Pathol.* 43 (1993) 343.
- [25] S. Oard, B.B. Karki, Mechanism of β -purothionin antimicrobial peptide inhibition by metal ions: molecular dynamics simulation study, *Biophys. Chem.* 121 (2006) 30.
- [26] S. Oard, B. Karki, F. Enright, Is there a difference in metal ion-based inhibition between members of thionin family: molecular dynamics simulation study, *Biophys. Chem.* 130 (2007) 65.
- [27] K. Matsuzaki, O. Murase, N. Fujii, K. Miyajima, An antimicrobial peptide, magainin 2, induced rapid flip-flop of phospholipids coupled with pore formation and peptide translocation, *Biochemistry* 35 (1996) 11361.
- [28] L. Yang, T. Harroun, T. Weiss, L. Ding, H. Huang, Barrel-stave model or toroidal model? A case study on melittin pores, *Biophys. J.* 81 (2001) 1475.
- [29] J. Wang, P. Cieplak, P.A. Kollman, How well does a restrained electrostatic potential (RESP) model perform in calculating conformational energies of organic and biological molecules? *J. Comput. Chem.* 21 (2000) 1049.
- [30] L.X. Dang, B.M. Pettitt, Simple intramolecular model potentials for water, *J. Phys. Chem.* 91 (1987) 3349.
- [31] W.L. Jorgensen, J.D. Madura, R.W. Impey, M.L. Klein, Comparison of simple potential functions for simulating liquid water, *J. Chem. Phys.* 79 (1983) 926.
- [32] H.J.C. Berendsen, J.R. Grigera, T.P. Straatsma, The missing term in effective pair potentials, *J. Phys. Chem.* 91 (1987) 6269.
- [33] H.W. Horn, W.C. Swope, J.W. Pitera, J.D. Madura, T.J. Dick, G.L. Hura, T. Head-Gordon, Development of an improved four-site water model for biomolecular simulations: TIP4P-Ew, *J. Chem. Phys.* 120 (2004) 9665.
- [34] A. Lyubartsev, A. Laaksonen, Osmotic and activity coefficients for effective potentials for hydrated ions, *Phys. Rev. E* 55 (1997) 5689.
- [35] I. Joung, T.R. Cheatham, Molecular dynamics simulations of the dynamic and energetic properties of alkali and halide ions using water-model-specific ion parameters, *J. Phys. Chem. B* 113 (2009) 13279.
- [36] T. Nemoto, M. Uebayasi, Y. Komeiji, Flexibility of a loop in a pheromone binding protein from *Bombyx mori*: a molecular dynamics simulation, *Chem-Bio. Info. J.* 2 (2002) 32.
- [37] T. Darden, D. York, L. Pedersen, Particle mesh Ewald: an $N \cdot \log(N)$ method for Ewald sums in large systems, *J. Chem. Phys.* 98 (1993) 10089.
- [38] Y. Komeiji, M. Uebayasi, Peach-Grape system — a high performance simulator for biomolecules, *Chem-Bio. Info. J.* 2 (2002) 102.
- [39] D.A. Pearlman, D.A. Case, J.W. Caldwell, W.R. Ross, I.T.E. Cheatham, S. DeBolt, D. Ferguson, G. Seibel, P.A. Kollman, AMBER, a computer program for applying molecular mechanics, normal mode analysis, molecular dynamics and free energy calculations to elucidate the structures and energies of molecules, *Comp. Phys. Commun.* 91 (1995) 1.
- [40] W. Humphrey, A. Dalke, K. Schulten, VMD: visual molecular dynamics, *J. Mol. Graph.* 14 (1996) 33.
- [41] W. Kabsch, C. Sander, Dictionary of protein secondary structure: pattern recognition of hydrogen-bonded and geometrical features, *Biopolymers* 22 (1983) 2577.
- [42] J.H. Friedman, Greedy function approximation: a gradient boosting machine, *Ann. Stat.* 29 (2001) 1189.
- [43] L. Breiman, J.H. Friedman, R.A. Olshen, C.J. Stone, *Classification and Regression Trees* Belmont, California, 1984.
- [44] R. Schapire, MSRI Workshop on Nonlinear Estimation and Classification M.H.H. in: D.D. Denison, C. Holmes, B. Mallick, B. Yu (Eds.), *The boosting approach to machine learning — an overview*, Springer, NY, 2003.
- [45] A. Grossfield, S. Feller, M. Pitman, Convergence of molecular dynamics simulations of membrane proteins, *Proteins* 67 (2007) 31.
- [46] K.A. Johnson, E. Kim, M.M. Teeter, S.W. Suh, B. Stec, Crystal structure of alpha-hordothionin at 1.9 Angstrom resolution, *FEBS Lett.* 579 (2005) 2301.
- [47] B. Stec, Plant thionins — the structural perspective, *Cell. Mol. Life Sci.* 63 (2006) 1370.
- [48] B. Bechinger, The structure, dynamics and orientation of antimicrobial peptides in membranes by multidimensional solid-state NMR spectroscopy, *Biochim. Biophys. Acta* 1462 (1999) 157.
- [49] F. Porcelli, B. Buck-Koehntop, S. Thennarasu, A. Ramamoorthy, G. Veglia, Structures of the dimeric and monomeric variants of magainin antimicrobial peptides (MSI-78 and MSI-594) in micelles and bilayers, determined by NMR spectroscopy, *Biochemistry* 45 (2006) 5793.
- [50] J.D. Lear, Z.R. Wasserman, W.F. DeGrado, Synthetic amphiphilic peptide models for protein ion channels, *Science* 240 (1988) 1177.
- [51] G.A. Woolley, R.M. Epand, I.D. Kerr, M.S. Sansom, B.A. Wallace, Alamethicin pyromellitate: an ion-activated channel-forming peptide, *Biochemistry* 33 (1994) 6850.
- [52] J. Aaira, M. Jelokhani-Niaraki, S. Osada, F. Kato, H. Kodama, Ion-channel formation assisted by electrostatic interhelical interactions in covalently dimerized amphiphilic helical peptides, *Biochemistry* 47 (2008) 3705.